Plasmonics (2006)
DOI 10.1007/s11468-005-9001-4

ORIGINAL PAPER

Dispersion Study of the Infrared Transmission Resonances of Freestanding Ni Microarrays

Shaun M. Williams · James V. Coe

Received: 24 February 2006 / Accepted: 10 March 2006

Abstract Nickel films (several-micrometer thickness, with 5.2-μm square holes in a square lattice array with 12.7-μm hole-to-hole spacing) exhibit Ebbesen's extraordinary transmission effect in the infrared; that is, they transmit a higher fraction of incident infrared light than the fractional open area of the holes. The role of surface plasmons (SPs) in this phenomenon is much debated, so we have obtained a data set whereby this idea and others can be tested against empirically determined dispersion curves. Unpolarized, zero-order transmission spectra have been recorded by rotating the mesh (from −2° to 60° in 1° steps) relative to the spectrometer's incident beam about an axis along the mesh's nearest hole-to-hole spacing in order to create the dispersion diagram. The data are numerically analyzed for peak centers that are then projected outside of the light line (by SP momentum matching equations) to two SP dispersion curves that are spaced in frequency by a splitting. With this caveat, all of the observed structure is accounted for by a simple SP model.

Key words Surface plasmons in the infrared · Nickel bigrating · Subwavelength apertures · Extraordinary transmission in the infrared · Thinness splitting

Introduction

The study of the optical properties of subwavelength apertures has become "one of the most exciting areas in optics research" [1]. In pursuit of such studies, it is noteworthy that freestanding nickel microarrays can be purchased commercially that exhibit Ebbesen's extraordinary transmission effect [2,3] in the infrared (IR) region of the electromagnetic spectrum [4,5]. A surface plasmon (SP)-mediated mechanism is generally cited as the means by which this increased transmission occurs. The biperiodic grating nature of the mesh couples with the incident light to produce an SP type of polariton [6] (oscillation of the metal's conducting electrons at the surface of the metal). The SPs propagate along the surface of the mesh, perhaps on both sides, to another hole where they decouple, producing photons that emerge with the same direction as the incident beam. Studies by other researchers have been made concerning ultrafast behavior [7], entangled photon [8], polarization effects [9], and SP propagation between separated microarrays [10]. These studies indicate the fundamental nature of the phenomena as a single-photon process [8] that can preserve phase [7] and polarization [11].

The present studies are interesting because the dielectric properties of metals are very different in the IR than in the visible region where much SP work occurs [9,12–15]. The effect on IR transmission of aperture shape and film thickness of metallic microarrays has also been studied [16–19]. The IR region has energies that match fundamental molecular vibrations, and IR absorption enhancements of more than 100 times have been reported for molecular surface species using these new phenomena [4,20–22]. Data recorded in this region can serve as a rigorous test of theories describing SP-mediated extraordinary transmission.

The complex dielectric properties of metals can support some interesting surface states at the interface between the metal and a dielectric. The dielectric constant of a metal is complex $\left(\varepsilon_m = \varepsilon'_m + i\varepsilon''_m\right)$ and SPs can be supported [6] on a semi-infinite, smooth air/metal interface if $\left|\varepsilon'_m\right| > \varepsilon''_m$. This condition is true for silver, gold, and copper at wavelengths longer than

S. M. Williams · J. V. Coe (✉)
Department of Chemistry,
The Ohio State University,
100 West 18th Avenue, Columbus, OH 43210-1173, USA
e-mail: coe.1@osu.edu

260, 500, and 338 nm, respectively (using the fit of experimental data to a Lorentz–Drude model made by Rakic et al. [12]). Consequently, these are the metals of choice for SP work in the visible. This condition becomes true for nickel at 2496 nm or 4006 cm^{-1}, so nickel will support SPs in the mid-IR. The Lorentz-Drude model value of Ni's dielectric is $-134 + i100$ at 3000 cm^{-1} and the value is $-2361 + i1466$ at 700 cm^{-1}, which is quite different than the visible region. For a smooth semi-infinite air/metal interface [6], propagating SP dispersion is defined by the effective index of refraction of the interface as

$$n'_{eff} = \Re e\left\{\sqrt{\frac{\varepsilon_m}{\varepsilon_m + 1}}\right\}. \quad (1)$$

A silver/air interface has $n'_{eff} = 1.41$ at 800 nm on the edge of the visible region, whereas $n'_{eff} = 1.00006$ at 700 cm^{-1} in the IR region. Similarly, Ni/air has $n'_{eff} = 1.00015$ at 700 cm^{-1}. One expects SP dispersion to follow the light line closely in the IR, so any observed deviation of the SP dispersion curve from the light line as in this work is interesting and deserving of attention.

In this work, a series of zero-order FTIR transmission spectra have been recorded with unpolarized light. Taking the z direction as perpendicular to the mesh (see Figure 1), the mesh was rotated at 1° increments (a 5-fold finer increment than with our original work [4]) about the y axis along the nearest hole-to-hole spacing of the square lattice and perpendicular to the spectrometer's incident beam (this is sometimes called the Γ–X direction). The component of incident light in the x direction is varied by this arrangement. This enabled the construction of a single dispersion image (as given in Figure 2) from all of the transmission spectra of different angles (θ) which could be analyzed numerically for transmission maxima. The finer angular sampling enables a more detailed analysis in k space and many more and different resonance peaks were identified that could not be identified by fitting resonances in the frequency space of the original recorded spectra. All of the identified resonance positions are projected onto a split set of dispersion curves outside the light line demonstrating the validity of the SP model. However, SPs are not the whole story: Some light goes directly through the holes, producing a small unstructured,

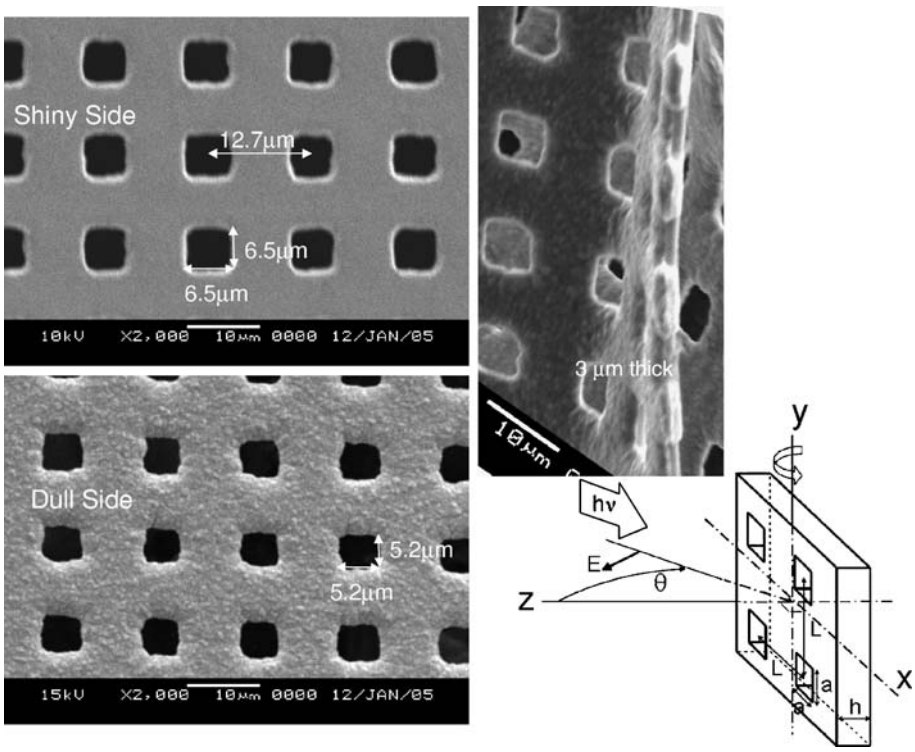

Figure 1. SEM microscope images of the nickel mesh. Top left, smooth side; bottom left, rough side. The smooth side has hole widths of ~6 μm whereas the rough side has hole widths of ~5 μm. Top right shows the mesh on edge that allows for the thickness of the mesh to be measured (~3 μm). The diagram in the lower right shows the geometry of the mesh and defines a coordinate system for discussions.

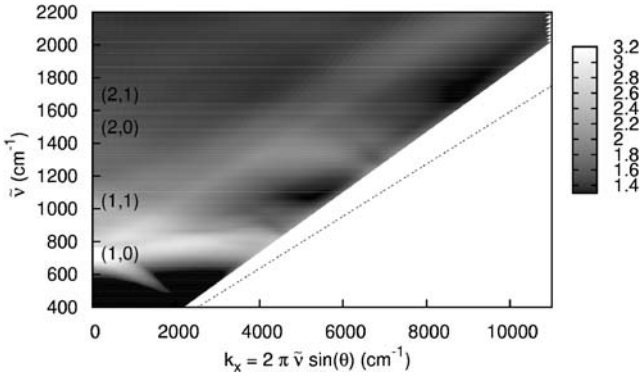

Figure 2. The dispersion of the IR transmission resonances for the Ni mesh. The natural logarithm of percent transmission ($\%T$) is presented as a function of photon wavenumber ($\widetilde{\nu}$) and momentum parallel to the surface (k_x). The light regions have a high transmission and the dark regions have a low transmission. The dark line is the "light line" which represents light impinging on the mesh from $\theta = 90°$, i.e., parallel to the surface. The $(|i|, |j|)$ identity of certain resonances is labeled at $k_x = 0$.

zero-order frequency spectrum (see Figure 1 in [23]); there are semantic issues concerning the definition of SPs [24], and there are issues in coupling the hole transmission to the SP picture. Additionally, Ebbesen's former coworkers (Thio and Lezec) favor composite diffracted evanescent waves [25], Moreno et al. [26] have suggested that the s-polarized features are not attributable to plasmons, and Garcia-Vidal et al. [1] have proposed geometrical surface states.

The dispersion curve of propagating SPs is said to "lie outside the light line" [6] (the line indicating the maximum momentum light can provide by traveling parallel to the surface) because SPs cannot be excited at a smooth air/metal interface simply by changing the angle of incident light. A coupling, typically by prisms, gratings, or surface roughness, is required to change the light's momentum sufficiently to excite the SPs. Square lattice biperiodic gratings can add or subtract momentum [2,6] in units of $(2\pi/L)i + (2\pi/L)j$, where i and j are integer steps along the reciprocal lattice (where i and j are taken in the x and y directions) and L is the hole-to-hole spacing of the array. There have been arguments as to the role of SPs in the Ebbesen effect [25,27,28], with many researchers considering SPs to be the primary cause of the effect, whereas a few others consider them secondary [24]. The exact nature of the SP's role for extraordinary transmission remains a challenging theoretical problem in optical physics [1,3,27]. Theory is not at the point where the lineshape of the observed transmission resonances can be reliably fit, although there has been some work on the most prominent resonance [3,4]. Consequently, we have set out to numerically analyze our transmission vs. angle data for transmission maxima. Transmission spectra are recorded with different components of light momentum parallel to the surface (by angling the mesh relative to the spectrometer's beam in the x direction) and a dispersion plot is constructed from which peak maxima are identified. Although typically one might extract peak centers from spectra vs. $\widetilde{\nu}$ (indicating wavenumbers that are proportional to energy as in conventional in IR spectroscopy), we are able to find many more peaks by analyzing spectra vs. the x component of momentum (k_x). Using (i,j) assignments (based on the observed positions of resonances relative to SP curve predictions assuming $n'_{eff} = 1.000$) and observed k_x values of resonances, we project outside of the light line by the left-hand side of the SP momentum matching equation:

$$\sqrt{\left(k_x + i\frac{2\pi}{L}\right)^2 + \left(j\frac{2\pi}{L}\right)^2} = \left|\vec{k}_{SP}\right| = n_{eff}(\widetilde{\nu})2\pi\widetilde{\nu}, \qquad (2)$$

where L is the hole-to-hole spacing. If $n_{eff}(\widetilde{\nu})$ is a slowly changing and/or simple function of $\widetilde{\nu}$, then Eq. (2) can be solved to obtain more refined SP curves of biperiodic mesh upon grating–coupling within the light line, which facilitates characterization of the bandgaps.

Experimental

The Ni mesh used is available from Precision Eforming (839 Route 13, Cortland, NY 13045, USA) in 15 × 15 cm sheets. Scanning electron microscope images reveal the geometry as shown in Figure 1. The mesh holes are arranged as a square lattice with a hole-to-hole spacing of 12.7 μm and a thickness of ~3 μm. The holes are primarily square in cross section, though the corners are rounded. Each hole has dimension of about 6.5 × 6.5 μm on the smooth side of the mesh which tapers to a minimum of about 5.2 × 5.2 μm towards the rougher side. Many of the details of the production of the mesh are proprietary, so the reader is directed to Precision Eforming for more specifics.

A piece of the Ni mesh was stretched over a stainless steel plate with a 2.54 cm aperture and secured to the plate. The plate was then placed in the sample position of a Mattson Cygnus 100 FTIR spectrometer and the zero-order transmission spectra were recorded. This plate was bolted to a small 360° rotating mount (model NT55-030, Edmund Industrial Optics, 101 E. Gloucester Pike, Barrington, NJ 08007-1380, USA), which was then affixed to the bottom of the sample compartment. This rotating mount allowed the mesh to be rotated relative to the incident spectrometer beam. The trans-

mitted diffraction pattern of a HeNe laser on the mesh was used to align one of the square lattice axes with the physical rotation axis. Transmission spectra were recorded in steps of 1° from $\theta = -2°$ to 60° relative to the mesh normal, where 0° corresponds to the incident beam being perpendicular to the surface of the mesh. The spectra were recorded using a 1-mm liquid-nitrogen-cooled MCT detector, at a resolution of 4 cm^{-1}, a spectral range of 400–5000 cm^{-1}, and a step size of 0.96435 cm^{-1}. Each spectrum is an average of 100 scans requiring ~1.72 min for each spectrum.

The data consisted of 63 spectra at different incident angles (θ), each with 4771 data points [percent transmission ($\%T$) vs. wavenumber ($\tilde{\nu}$)]. The momentum parallel to the surface (k_x) is calculated as $2\pi\tilde{\nu}\sin\theta$ at each point in each spectra. All of the data are presented as a 3-D plot in Figure 2 with $\%T$ (on a natural log scale where black is low transmission and white is high transmission) vs. $\tilde{\nu}$ and k_x. At perpendicular incidence ($\theta = 0$, $k_x = 0$), the primary resonance occurs at 728.1 cm^{-1} with a transmission of 80.6%. The maximum possible angle is 90°, which corresponds to the incident light's momentum being completely parallel to the surface, as indicated by the black line in Figure 2 (known as the "light line"). The resonances are labeled as with earlier work [4,29] by $(|i|, |j|)$, which are integer steps along the reciprocal lattice. As this notation also labels diffraction spots, these resonances can be thought of as occurring at the wavelength where each diffraction spot is no longer being transmitted [30] and is instead being trapped as evanescent waves along the surface. The primary resonance, labeled as (1,0) in Figure 2, is actually a combination of the (±1,0) and (0,±1) resonances at normal incidence. Due to the square configuration of the hole array, this primary resonance can be expected [4] to break into three branches, (−1,0), (1,0), and (0,±1), as the value of k_x is increased. The (−1,0) peak disperses to lower wavenumbers toward the free electron curve from its $k_x = 0$ position at 728.1 cm^{-1}. The (−1,0) resonance is more isolated than any of the other resonances and therefore is the most easily examined. The (−1,0) resonance has previously been fit to a damped harmonic oscillator model [4] with some interesting results, but it has been hard to obtain similar fits of the higher energy features.

Results

The Ni mesh is optically thick (~3 μm) and has an open area of only 16.8%. This means that Ebbesen's extraordinary transmission effect is definitely present for this mesh as indicated by the maximum transmission of 80.6% [for the (1,0) resonance at normal incidence, as labeled in Figure 1]. This amount of transmission is a factor of 4.8 greater than an "ideal" transmission (transmission of only the light incident on holes). This means that the transmission is dominated by light that is incident on the metal yet still transmitted.

Traces of the (−1,0) resonance vs. angle at several chosen wavelengths are displayed in Figure 3 in order to present this data in a format more similar to fixed-wavelength, prism-coupled attenuated total reflection (ATR) measurements, which have been at the core of much SP work. These traces and all of the data sets were corrected for loss of incident light due to aperture angling by dividing the $\%T$ by $\cos(\theta)$. These transmission vs. angle curves have asymmetric lineshapes like ATR curves, but much broader linewidths than intrinsically limited ATR curves. The linewidths have previously been characterized by us [4,5] (in frequency space) as proportional to $e^{(0.173\mu m^{-1})(\lambda\mu m)}$, but this formula is more illuminating if rewritten as $e^{(\lambda\mu m)/(5.78\mu m)}$, i.e., the constant is the hole size. This suggests that the linewidths are limited by radiation damping as governed by transmission through the holes rather than mechanisms often associated with SPs propagating on nonperforated metal surfaces. Although propagating SPs are capable of traveling distances much greater than the lattice spacing on nonperforated metal surfaces, these SPs basically travel to the next hole where they couple out as light.

Resonance peak centers (k_x,$\tilde{\nu}$ pairs) are shown in Figure 4 that have been identified by evaluating the numerical second derivatives $\partial^2\%T/\partial k_x^2$ and $\partial^2\%T/\partial\tilde{\nu}^2$. Negative maxima in the second derivatives

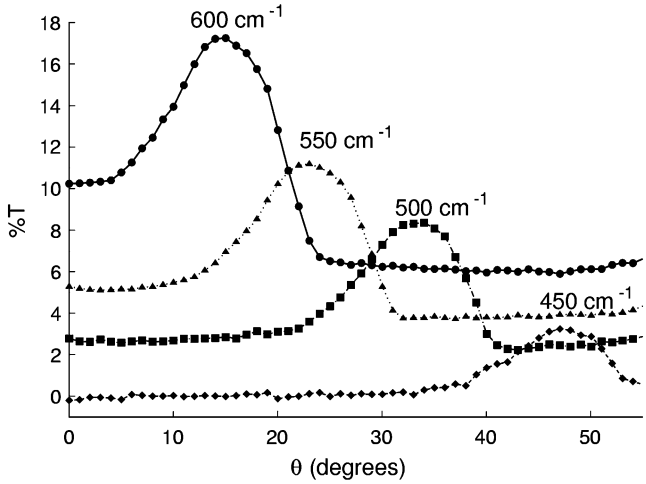

Figure 3. Traces of the (−1,0) resonance vs. angle at selected wavenumbers. These correspond to slices of the dispersion

correspond to the peak centers of the upward-going $\%T$ peaks. The $\partial^2\%T/\partial\tilde{\nu}^2$ data were very sensitive to the small contributions of rotationally resolved background gases, so all 63 spectra vs. $\tilde{\nu}$ had their high frequencies filtered by fast Fourier transformation using cutoffs that greatly eliminated the highly structured spectra of the background gases without noticeable effect on the resonance lineshapes (with particular attention to preventing alteration of the band gap structure). The $\partial^2\%T/\partial k_x^2$ data set only had 63 steps in k_x and was immune to the background spectra, but required two stages of five-point Sovitsky-Golay smoothing [31] to better establish the resonance positions. The open circles in Figure 4 are due to the second derivatives with respect to $\tilde{\nu}$, and the crosses are due to the second derivatives with respect to k_x. The k_x and $\tilde{\nu}$ second derivatives have very different sensitivities for the extraction of peak positions. The second derivative with respect to k_x better identifies peaks that follow the slope of the light line, which are barely evident in any of the 63 raw frequency spectra. Once the k_x values of the peak positions were extracted and assigned (i,j) resonance labels, these quantities were used with the left-hand side of Eq. (2) to predict the SP momentum outside of the light line. The results are presented in Figure 5.

There are two curves in Figure 5 with the simple form of $\tilde{\nu} = k_x \Big/ \left(2\pi n'_{eff}\right)$. One follows the light line (n'_{eff} = 1.000), whereas the other has been fit to a constant value of n'_{eff} = 1.061 ± 0.021. Substitution of this equation into Eq. (2) and solving for $\tilde{\nu}$, when n'_{eff} is constant, gives rise to the grating-coupled SP dispersion curves within the light line as

$$\nu_{i,j}(k_x) = \frac{\sqrt{\left(\frac{k_x}{2\pi} + \frac{i}{L}\right)^2 + \left(\frac{j}{L}\right)^2}}{n'_{eff}}. \qquad (3)$$

These curves are drawn in Figure 4 with dotted lines for n'_{eff} = 1.000 and solid lines for n'_{eff} = 1.061.

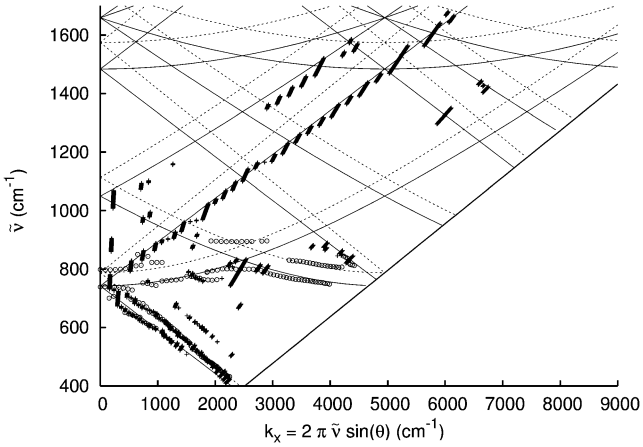

Figure 4. Dispersion plot of the peak centers found by examination of the second derivatives of transmission with respect to k_x and $\tilde{\nu}$. The open circles symbols come from the analysis with respect to $\tilde{\nu}$ and the cross symbols come from analysis with respect to k_x. The dispersion curve lines come from Eq. (3). Data in the (+1,0) and (+1,+1) branches extends several thousand wavenumbers higher, but this scale enables a closer examination of the lowest energy resonances. The solid lines correspond to the lower levels and the more displaced data set in Figure 5 with n'_{eff} = 1.061, whereas the dotted lines correspond to upper levels and points near the light line in Figure 5.

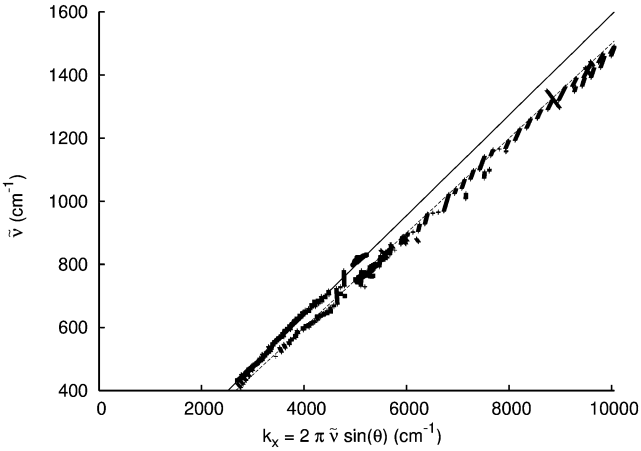

Figure 5. SP dispersion curves lying outside the light line, which are grating-coupled to the curves of Figure 4. The points away from bandgaps in Figure 4 have been translated outside of the light line (solid line) by the angular momentum matching formula of the left-hand side of Eq. (2). The points group into two sets: one that follows the light line (n'_{eff} = 1.000) and one that is modeled with n'_{eff} = 1.061 using a dotted line.

Discussion

One of the sets in Figure 5 lies on the light line, as predicted by Eq. (1) for a nonperforated Ni/air interface, while the other is significantly displaced from the light line. In our frequency spectra, the resonance feature below the bandgap is considerably larger than the corresponding feature above the gap. Consequently, it was easier to pick up features in this analysis from below the bandgap, as is evident by the more complete representation of the more displaced curve in Figure 5.

Bigratings are different and more complicated than 1-D gratings. On a bigrating, SPs can propagate equally well along the holes in either of two perpendicular directions (the x or y directions). Note that SPs in both directions are each like the p-polarized SPs on 1-D gratings. If we rotate about the y axis, SPs traveling in the x direction [such as the (±1,0) branches] see different x components of the light and disperse

like normal p-polarized SPs. However, SPs propagating in the y direction [such as the (0,±1) branches] do not see changes in the y component of the light and do not disperse like the x components. Barnes et al. [9] (and our own polarized work to be published shortly) have shown that the (0,±1) branch exhibits an initially flat dispersion curve and s polarization, whereas the (±1,0) branches are p polarized. The s-polarized behavior of these SPs, such as the (0,±1) modes, can be predicted by Eq. (3). If the effective dielectric constant of the perforated system is constant in $\widetilde{\nu}$, then an expansion predicts quadratic behavior [4] in k_x:

$$\widetilde{\nu}_{0,\pm1}(k_x) = \frac{1}{Ln'_{eff}} + \frac{L}{8\pi^2 n'_{eff}} k_x^2 + \ldots . \tag{4}$$

This quadratic behavior is readily evident in Figure 4. A theory and useful perspective has been put forward by Garcia-Vidaletal.[1] that deals with the dispersion of 2-D metallic arrays of holes with analogies to effective thin coatings, i.e., a smooth anisotropic layer on a perfect conductor. It is similar or perhaps based on a theory by Martin-Moreno et al. [3], which consider the holes as waveguides. The latter predicts lineshapes, but it does not contain explicit dispersion effects, rather it deals with normally incident light. The theory of Garcia-Vidal et al. includes thickness and offers a dispersion relation [1]. It predicts a very flat dispersion in the region of our primary resonance, but it is based on p-polarized light, and our (0,±1) features are observed with s polarization. Also, the predicted dispersion curve bends downward as its flattens with increasing k_x, whereas the observed curve is quadratically upward. The evidence in this case points to propagating SPs rather than a geometric surface state.

Displacement from the light line was identified by Lezec and Thio [25] as an important observation contributing to their development of an alternative explanation to SPs based on a composite evanescent diffraction model; however, an SP explanation has become apparent. The two curves in Figure 5 represent features just above and below a gap or splitting. The spacing between the two curves in Figure 5 in frequency space (vertically in Figure 5) shows that the value of the splitting gets larger at higher energies. Very thin metal films give rise to two dispersion curves (sometimes designated ω_- and ω_+), which split above and below the semi-infinite dispersion curve [6]. As the thickness is increased, this split from the semi-infinite dispersion curve decreases. Although our mesh is fairly thick [~3 μm as compared to a 14-μm wavelength at the (1,0) resonance], one likely possibility is that the coupling of the front and back surfaces by holes is similar to the splitting associated with thinness.

A line midway between the two curves ($n'_{eff} = 1.03$) would indicate the band centers (or the semi-infinite curve) and it is detectably off of the light line. If this analysis holds up to future scrutiny, then the band centers are different from expectations based on SP propagation on smooth air/metal interfaces. One possible explanation might involve the transmission process through the hole (we already know that the hole width is limiting the lifetimes).

It was brought to our attention that the true peak centers could have different positions than the maxima of transmission spectra. In our first paper dealing with Ni mesh [4], we were able to fit the isolated (−1,0) resonance to a damped harmonic oscillator model, so the fits were examined to see the direction and magnitude of such an effect. At $\theta = 40°$, the fitted resonance center occurred at 450 cm^{-1}, while the transmission peak was maximum at 470 cm^{-1}. So, the differences are small, on the order of 20 cm^{-1}, and the direction of the true resonance energy is either shifted along the SP dispersion curve or shifted even further from the light line than indicated by the numerical transmission peak centers of this work. Consequently, the differences between transmission peak centers and true resonance positions are not expected to effect our conclusions about n_{eff}.

In conclusion, Ni mesh with square holes arranged in a square lattice shows the same extraordinary transmission in the IR that has been primarily seen in the visible. The dispersion curve of the resonances (see Figure 5) shows a splitting that is likely related to the tunneling through subwavelength holes. There is a 3% difference from the light line to the center of these splittings that is much larger than expected by SPs on nonperforated, smooth metal/air interfaces. Again this may be indicative of light passing through the holes rather than propagating along the front and back surfaces. In practice, the radiation-damped [32] resonance lineshapes become quite distorted when close to the bandgaps. It would be very useful to have a theory of the lineshapes for fitting that is valid near the bandgaps. Hopefully, these data will encourage the development of improved theories which in turn will aid in the development of more applications of these interesting phenomena.

Acknowledgements We thank the ACS PRF 38502-ACS and the NSF CHE0413077 for support.

References

1. Garcia-Vidal FJ et al (2005) Surfaces with holes in them: new plasmonic metamaterials. J Opt A 7:S97–S101

2. Ebbesen TW et al (1998) Extraordinary optical transmission through sub-wavelength hole arrays. Nature (Lond.) 391(6668):667–669
3. Martin-Moreno L et al (2001) Theory of extraordinary optical transmission through subwavelength hole arrays. Phys Rev Lett 86(6):1114–1117
4. Williams SM et al (2003) Accessing surface plasmons with Ni microarrays for enhanced IR absorption by monolayers. J Phys Chem B 107(43):11871–11879
5. Williams SM et al (2004) Scaffolding for nanotechnology: extraordinary infrared transmission of metallic microarrays for stacked sensors and surface spectroscopy. Nanotechnology 15:S495–S503
6. Raether H (1988) Surface Plasmons on Smooth and Rough Surfaces and on Gratings, Springer-Verlag, Berlin
7. Dogariu A et al (2001) Delay in light transmission through small apertures. Opt Lett 26(7):450–452
8. Altewischer E et al (2002) Plasmon-assisted transmission of entangled photons. Nature (Lond.) 418(6895):304–306
9. Barnes WL et al (2004) Surface plasmon polaritons and their role in the enhanced transmission of light through periodic arrays of subwavelength holes in a metal film. Phys Rev Lett 92(10):107401–107405
10. Devaux E et al (2003) Launching and decoupling surface plasmons via micro-gratings. Appl Phys Lett 83(24):4936–4938
11. Altewischer E et al (2005) Polarization tomography of metallic nanohole arrays. Opt Lett 30(1):90–92
12. Rakic AD et al (1998) Optical properties of metallic films for vertical-cavity optoelectronic devices. Appl Opt 37(22): 5271–5283
13. Krishnan A et al (2001) Evanescently coupled resonance in surface plasmon enhanced transmission. Opt Commun 200(1–6):1–7
14. Degiron A et al (2002) Effects of hole depth on enhanced light transmission through subwavelength hole arrays. Appl Phys Lett 81(23):4327–4329
15. Barnes WL et al (2003) Surface plasmon subwavelength optics. Nature (Lond.) 424(6950):824–830
16. Moller KD et al (1999) Thin and thick cross shaped metal grids. Infrared Phys Technol 40(6):475–485
17. van der Molen KL et al (2005) Role of shape and localized resonances in extraordinary transmission through periodic arrays of subwavelength holes: experiment and theory. Phys Rev B 72(4):045421/1–045421/9
18. Koerkamp KJK et al (2004) Strong influence of hole shape on extraordinary transmission through periodic arrays of subwavelength holes. Phys Rev Lett 92(18):183901/1–183901/4
19. Gordon R et al (2005) Basis and lattice polarization mechanisms for light transmission through nanohole arrays in a metal film. Nano Lett 5(7):1243–1246
20. Williams SM et al (2004) Use of the extraordinary infrared transmission of metallic subwavelength arrays to study the catalyzed reaction of methanol to formaldehyde on copper oxide. J Phys Chem B 108(31):11833–11837
21. Williams SM et al (2004) Scaffolding for nanotechnology: extraordinary IR transmission of metal microarrays for stacked sensors and surface spectroscopy. Nanotechnology 15(10):S495–S503
22. Rodriguez KR et al (2004) Enhanced infrared absorption spectra of self-assembled alkanethiol monolayers using the extraordinary infrared transmission of metallic arrays of subwavelength apertures. J Chem Phys 121(18):8671–8675
23. Williams SM et al (2004) Use of the extraordinary transmission of metallic subwavelength arrays to study the catalyzed reaction of methanol to formaldehyde on copper oxide. J Phys Chem B 108:11833–11837
24. Treacy MMJ (2002) Dynamical diffraction explanation of the anomalous transmission of light through metallic gratings. Phys Rev B 66(195105):1–11
25. Lezec HJ, Thio T (2004) Diffracted evanescent wave model for enhanced and suppressed optical transmission through subwavelength hole arrays. Opt Express 12(16):3269–3651
26. Moreno E et al (2005) Extraordinary optical transmission without plasmons: the s-polarization case. Los Alamos National Laboratory, Preprint Archive, Condensed Matter 1–4, arXiv:cond-mat/0502089
27. Popov E et al (2000) Theory of light transmission through subwavelength periodic hole arrays. Phys Rev B 62(23): 16100–16108
28. Cao Q, Lalanne P (2002) Negative role of surface plasmons in the transmission of metallic gratings with very narrow slits. Phys Rev Lett 88(57403):1–4
29. Ghaemi HF et al (1998) Surface plasmons enhance optical transmission through subwavelength holes. Phys Rev B 58(11):6779–6782
30. Vigoureux JM (2001) Analysis of the Ebbesen experiment in the light of evanescent short range diffraction. Opt Commun 198(4–6):257–263
31. Press WH et al (1992) Numerical Recipes in Fortran 77: The Art of Scientific Computing, Cambridge University Press, Cambridge
32. Naweed A et al (2003) Evidence for radiative damping in surface-plasmon-mediated light transmission through perforated conducting films. J Opt Soc Am B: Opt Phys 20(12):2534–2538